Sensors and Materials, Vol. 12, No. 3 (2000) 143–162
MYU Tokyo

S & M 0404

Fabrication Process for High *Q* Polysilicon Beam Resonators

Yongchul Ahn and Henry Guckel

Wisconsin Center for Applied Microelectronics,
Department of Electrical and Computer Engineering,
University of Wisconsin-Madison,
1410 Engineering Dr., Madison, WI 53706, U.S.A.

(Received November 1, 1999; accepted April 14, 2000)

Key words: polysilicon, sensor, resonator, vacuum cavity, surface micromachining

The fabrication process for polysilicon beam resonators is presented. The methodology is based on a two-level polysilicon process via surface micromachining technology. This approach has led to a family of high *Q* polysilicon resonators which are now being used for the measurement of physical variables which can be converted to axial strain via an appropriate silicon microstructure by measuring strain induced changes of resonant frequencies. This type of resonator typically involves a clamped-clamped beam located in a vacuum cavity and electronic driving and sensing components. The freeing of microstructures in the cavity is established by freezing and sublimation processes. The cavity vacuum is produced by LPCVD polysilicon sealing. Long-term vacuum integrity is achieved by a low-stress silicon nitride barrier which also behaves as an interdielectric layer. The electronic driving and sensing components are fabricated using a standard IC fabrication technology. Experimental results of dynamic mechanical responses of these devices are presented. Measured performance indicates typical resonant frequencies of several hundred kilohertz (kHz) with quality factors as large as 300,000.

1. Introduction

Micromachined polysilicon beam resonators are used in sensors which can measure parameters such as pressure, temperature, force, and acceleration. These devices transduce via changes in resonant frequencies when they are subjected to an axial strain variation due to changes in these parameters.[1–6]

Micromachined beam resonators can be fabricated using a planar microfabrication process. Micromechanical beams inside sealed vacuum cavities are produced by surface micromachining techniques. The hard vacuum environment yields high quality factor, Q, resonators. The fabrication process for microbeam resonators is also influenced by the choice of excitation schemes and the electrical readout circuitry.

J. J. Sniegowski[4] at the University of Wisconsin-Madison developed the encapsulated clamped-clamped microbeams in vacuum using a two-level polysilicon process. His microbeams were driven capacitively and sensed with polysilicon piezoresistors. Resonating microbeams have been further developed by changing the sensing schemes to optical and magnetic-field sensing methods.[6,7]

To obtain repeatable high Q devices with good yield, an understanding of the fabrication techniques for polysilicon beam resonators is essential. The fabrication techniques include polysilicon depositions with controlled microstructure, sublimation to prevent sticking[4] and sealing processes for cavity vacuum. Standard silicon processing techniques such as oxidation, implantation, photolithography, dry and wet etching, and thin film deposition are also involved. The fabrication techniques must be repeatable and stable with accurate process monitoring. The fabrication techniques for the polysilicon beam resonators were developed some time ago.[4,7] They required improvement and stabilization to obtain high Q devices and to increase device yields. The decision to use electrostatic excitation and detection in the polysilicon beam resonator required a modified processing sequence.

This paper describes the fabrication process of micromachined high Q polysilicon beam resonators with capacitive driving and sensing schemes. The fabrication of micromachined sealed vacuum cavities and the mechanical properties of polysilicon films are discussed. Design considerations for microbeams such as microbeam dimensions and electronic circuitry are considered. The fabrication sequence for microbeams and the layout of test chips are described. Experimental results such as resonant frequency and quality factor are also presented.

2. Micromachined Sealed Vacuum Cavities

The surface micromachining process for fabricating vacuum sealed cavities in polysilicon was developed and described by Guckel and Burns.[8,9] Figure 1 illustrates the simple procedure for making micromachined sealed vacuum cavities in polysilicon.[8,9] A thin silicon dioxide layer is initially grown and a low stress thin LPCVD silicon nitride layer is deposited on the wafer. The first masking step opens windows in the silicon dioxide and nitride at the cavity areas and is followed by a local oxidation of the opened silicon areas in

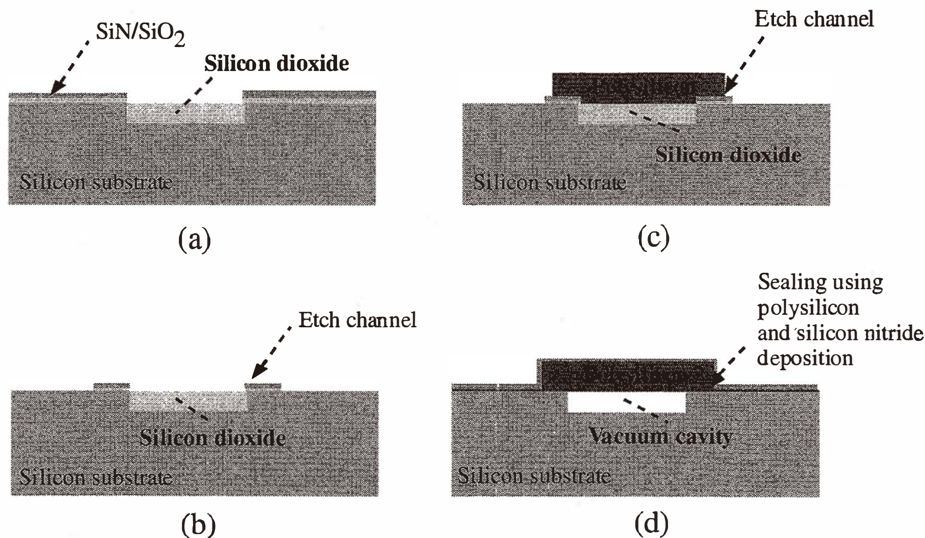

Fig. 1. Fabrication sequence of micromachined sealed vacuum cavity.

Fig. 1(a). Etch channels are then defined by plasma etching of the remaining silicon nitride/dioxide sandwich surrounding the cavity areas in the second masking step shown in Fig. 1(b). Polysilicon is deposited on the top of the silicon dioxide layer and the etch channels by low-pressure chemical vapor deposition (LPCVD) and patterned by plasma etching in the third masking step in Fig. 1(c). Immersing the wafer in hydrofluoric acid (HF) diluted by deionized (DI) water in the ratio of 1 to 1 removes all the silicon dioxide in the thin etch channels and under the polysilicon layer. The procedure is followed by a rinsing sequence. To avoid the effects of surface tension during drying, the final rinse liquid is removed by freezing followed by sublimation.[4,7,8] The vacuum inside the cavity is chemically induced as part of the reactive sealing process[4,6–8,10,11] as illustrated in Fig. 1(d). Several different reactive seals have been used, including oxygen, LPCVD silicon nitride, and polysilicon deposition,[4,7–9] as well as nonreactive seals using deposited metal films.[10] Procedures similar to this have been adapted to produce polysilicon resonating beam structures.[4,7]

Several aspects of reactive sealing using the decomposition of silane (SiH_4) to deposit polysilicon merit additional discussion.[10] The vacuum in the cavity is the result of the out-diffusion of hydrogen from the cavity following the polysilicon sealing step. Since the diffusion coefficient for hydrogen in polysilicon is large, this occurs quite rapidly in the LPCVD process. To prevent the diffusion of hydrogen and helium from the operating ambient, the devices are coated with a silicon nitride film.

3. Mechanical Properties of Polycrystalline Silicon

Proper design of polysilicon microstructures requires knowledge of the material properties of polysilicon such as Young's modulus, Poisson's ratio, the thermal expansion coefficient and the built-in strain. Problems with buckling or unwanted deflections of polysilicon microstructures are usually caused by the built-in strain of the polysilicon film. Therefore, it is important to establish the requirements for a reliable polycrystalline silicon process to make mechanical microstructures.

Polysilicon can have many forms when it is LPCVD-deposited from silane. For depositions near 580°C a very fine grained silicon film is obtained, whereas depositions near 640°C produce rather coarse grained films. Both films as-deposited normally produce compressive strains which may be as high as 2%. This can cause buckling in polysilicon microbeams. The control of the built-in strain in polysilicon films by annealing at several high temperatures was studied at the University of Wisconsin-Madison.[11] The results are shown in Fig. 2. A carefully designed annealing procedure can reduce the compressive strain significantly. In the case of fine grained polysilicon, annealing at moderate tempera-

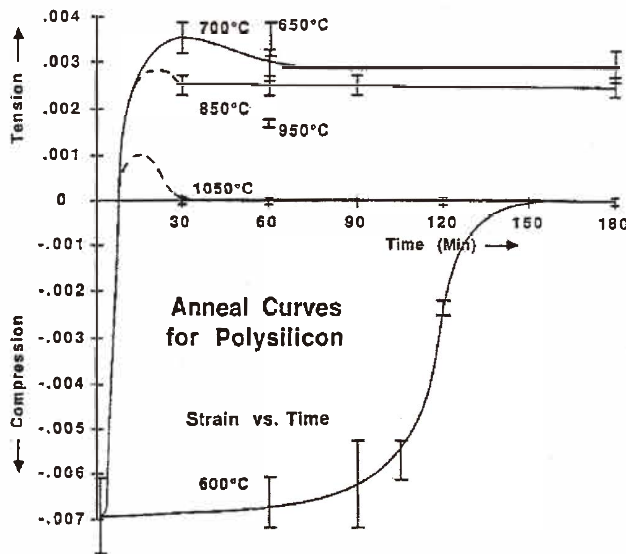

Fig. 2. Internal strain for LPCVD polysilicon films deposited on oxidized silicon substrates as a function of post-deposition annealing time and temperature. These films were deposited using the pyrolysis of 100% silane at a temperature of 580°C and a pressure of 300 mTorr.[11]

tures results in high tensile strain and annealing at high temperatures results in nearly zero strain without increase of the grain size. Polysilicon films with compressive tensile, and zero strains have been made.

Various measurements of the mechanical properties of polysilicon films lead to the following:

· Thickness tolerance: ±1%
· Young's modulus: $E = 1.62 \times 10^{12}$ dynes/cm^2
· Poisson's ratio: $\nu = 0.228$
· Built-in strain, ε_o: $0\% < \varepsilon_o < 0.3\%$ after annealing
· Temperature behavior of Young's modulus: –55 ppm/°C

If polysilicon is annealed at 825°C in nitrogen for 3 h, it becomes mechanically and optically indistinguishable from single crystal silicon, which is known for its excellent mechanical properties and stability. Thus, polysilicon microbeam structures can provide the basis for highly stable sensors and electromechanical actuators.

4. Design

4.1 *Beam shapes and dimensions*

Two different beam shapes are used in the design: a straight beam and an H-beam. Both are utilized as clamped-clamped beams resonating in the flexural mode. Simple diagrams of these beam configurations are shown in Fig. 3. The clamped-clamped straight beams have been the primary beam types selected for the development of beam resonators.[4,7] They are relatively easy to fabricate and amenable to several driving and sensing schemes. An H-shaped beam (H-beam) has also been used for the beam design. This structure was introduced by Yokogawa.[12] In this design, the size of the center mass connected with four legs is larger than that of Yokogawa's H-beam. There is a fairly large capacitance between electrodes, which allows the device to be operated as a one-port or a two-port sensor with capacitive driving and sensing capability.

The beam dimensions such as the beam length, width and thickness are determined by

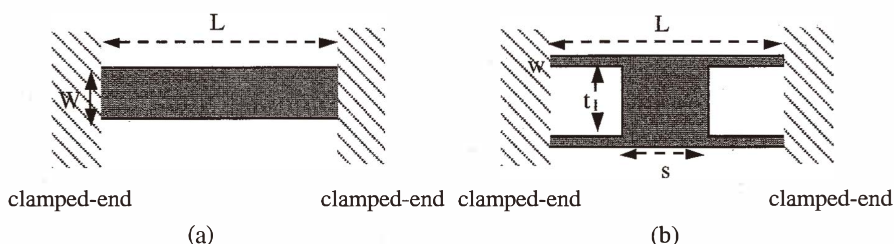

Fig. 3. The beam configurations: (a) a straight beam; (b) an H-Beam.

the choice of the nominal resonant frequency of the unloaded beam. In the beam resonators, relatively high frequency output is desirable for fast response time, for averaging the effects of vibrations, and for mechanical isolation. Data on the exact beam dimensions and measurements of the resonant frequencies can also be used for the evaluation of the mechanical properties of the beam material, such as Young's modulus and built-in strain. In this design, various beam lengths are chosen to get resonant frequencies of greater than 200 kHz from the beam resonators. Other parameters such as the beam width and thickness are kept constant.

4.2 *Cover dimensions*

The polysilicon cover and the silicon substrate form the vacuum cavity which contains the polysilicon beam in the resonating devices. Since the vacuum cavity encapsulated by the polysilicon cover provides a hard vacuum environment, the cover must be sufficiently rigid not to be destroyed by atmospheric pressure. Its rigidity depends on the cover dimensions such as length, width, thickness and the material properties. The cover length and width are determined by the dimensions of the upper sacrificial layers in the design. The cover thickness can be controlled in the process. Since the design involves H-beams which results in a very large area of the cover, an investigation of the deflection of the cover due to atmospheric pressure as a function of its dimensions is required. The equations to calculate the deflection, X_d of the cover due to atmospheric pressure follow those of plates for pressure transducers.[9] For a square plate with a side of length A, the governing equation is given by

$$X_d = (0.00126\,PA^4/D)/[1 + 9\,(1 + \nu)\,\varepsilon A^2/4\pi^2 h^2], \tag{1}$$

where $D = Eh^3/12(1 - \nu)^2$, E is Young's modulus, ν is Poisson's ratio, P is pressure, ε is the built-in strain, and h is the thickness. For a long rectangular plate having a width of W, the governing equation becomes

$$X_d = (0.00260\;PW^4/D)/[1+3(1+\nu)\varepsilon W^2/\pi^2 h^2], \tag{2}$$

where the parameters are the same as those in eq. (1) except for the width, W. Since the H-beams and the straight beams are approximated as square and long rectangular plates, respectively, both eqs. (1) and (2) can be used to determine the cover dimensions. Figure 4 shows the minimum dimensions for each case as functions of the cover size and thickness. If the design allows about 0.1 μm for the minimum deflection, as shown in Fig. 4, the design conditions for the cover are that the square plate size must be designed to be less than 150 μm in length with a thickness of 3.0 μm for an H-beam. The width cannot exceed 120 μm with a thickness of 3.0 μm for a straight beam.

4.3 *Driving and sensing structures*

The design of the electrostatically driven resonating beams includes a clamped-clamped beam sealed in a vacuum cavity and electronic components for driving and sensing. The driving and sensing mechanisms consist of capacitively-coupled electrode pairs in the

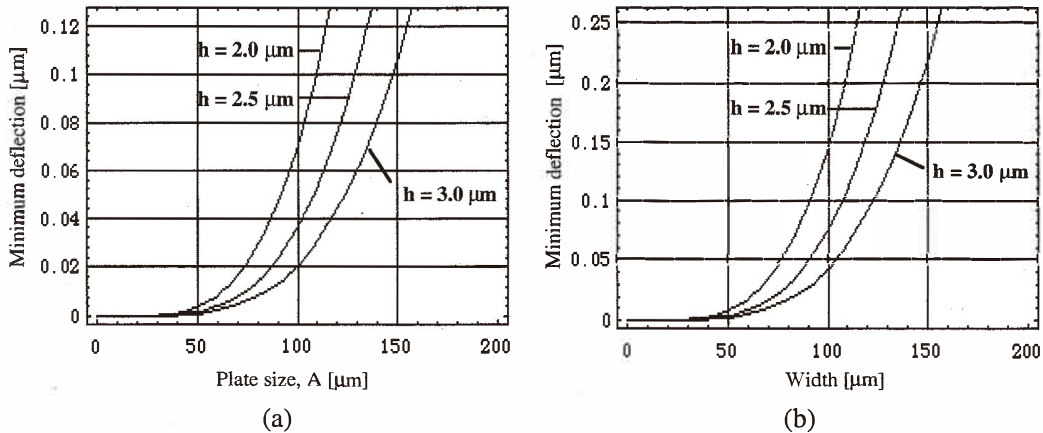

Fig. 4. Calculation of the minimum deflection of the polysilicon cover due to atmospheric pressure as functions of its size. No built-in strain in the polysilicon film is assumed: (a) for a square plate; (b) for a long rectangular plate.

device. These electrode pairs can be implemented with diffused layers in the silicon substrate, doped polysilicon resistors, and metal layers. The size and geometry of the driving and sensing electrodes depend on the application, but they are usually modeled as parallel-plate capacitors.

There are two types of beam resonator designs depending on driving and sensing operations: one-port and two-port beam resonators. The one-port beam resonators have one parallel-plate capacitor, so the driving and sensing operations are performed by the same electrode pair. Since the driving and sensing signals in these devices are coupled during operation, a fairly large capacitor is required to increase the sensitivity. Figure 5 shows the vertical cross-section of a one-port beam resonator. A parallel-plate capacitor in the device can be formed by the diffused layer in the silicon substrate and the doped beam polysilicon. The two-port beam resonators have a separate driving and sensing schemes. The coupling factor between the driving and sensing signals is presumed to be low. The two-port beam resonators can be implemented with the two different designs shown in Fig. 6.

In Fig. 7 layouts illustrate two types of microbeams: a straight beam and an H-beam. For H-beams, the one-port devices are referred to as HO. Two-port devices are designed as the two types shown in Fig. 6.

- One is referred to as HA with two separate boron diffused layers in the n-substrate for driving and sensing.
- The other is referred to as HB with a boron diffused layer in the n-substrate for driving and a metal layer on the polysilicon cover for sensing.

Similar notation applies to straight beams for two-port devices: SA with driving and sensing electrodes in the substrate, and SB with a diffused layer in the substrate for the driving electrode and a metal layer for the sensing electrode. Their dimensions such as length and width are varied as shown in Fig. 8. The driving and sensing electrode sizes of the devices fabricated with this design are listed in Table 1.

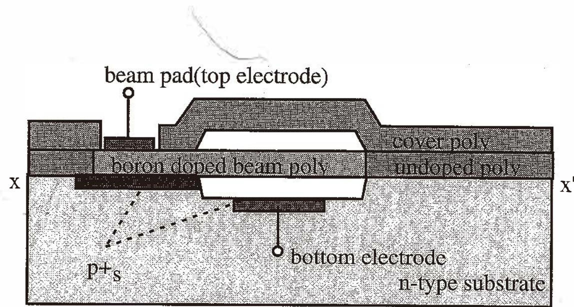

Fig. 5. Cross-sectional view of a one-port beam resonator. Two electrodes, the p+ diffused layer in the n-type silicon substrate and the boron doped beam polysilicon, form the parallel-plate capacitor.

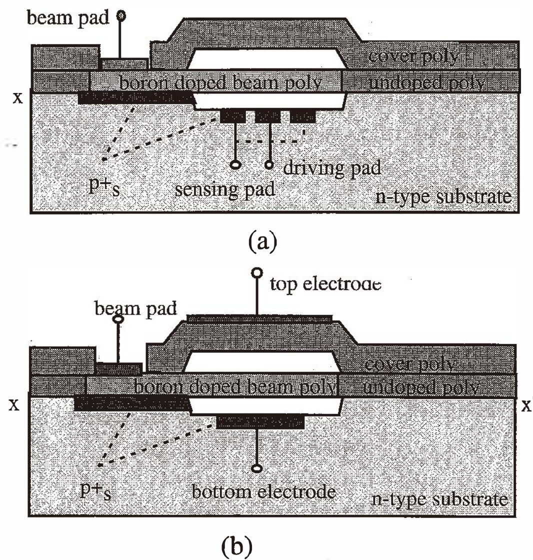

Fig. 6. Cross-sectional view of a two-port beam resonator which has two separate parallel-plate capacitors for driving and sensing: (a) Design A (b) Design B.

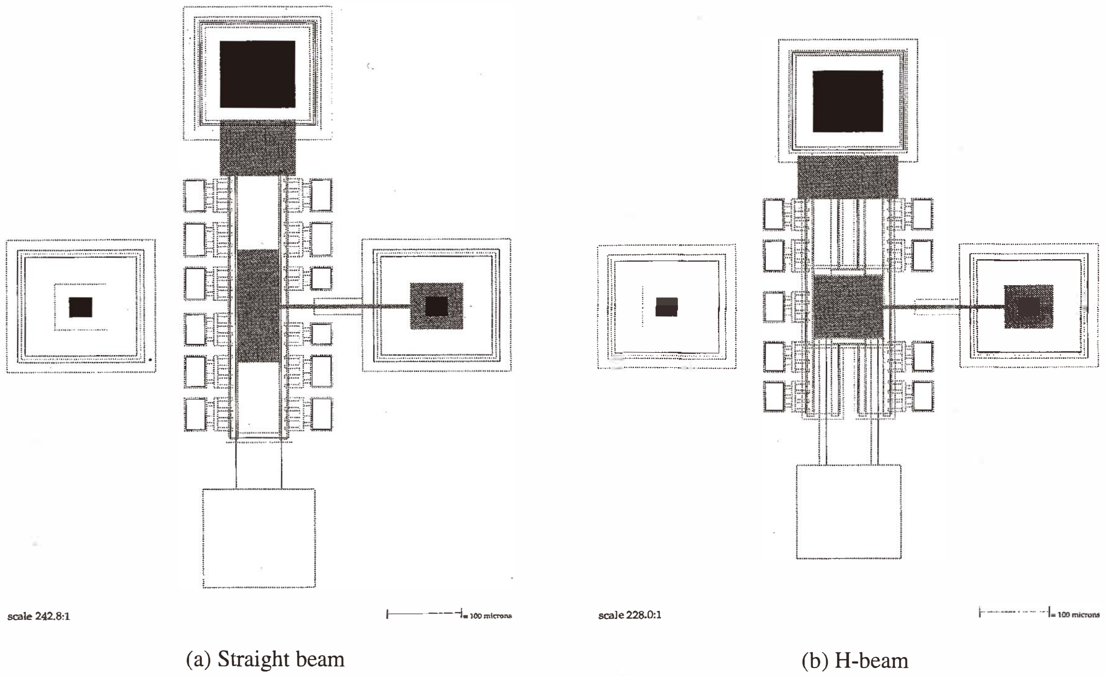

(a) Straight beam (b) H-beam

Fig.7. Layouts of microbeams.

Beam length, L	Beam width, W
300 µm 400 µm 500 µm	56 µm

(a)

Length, L	Leg width, b,	Diaphragm,
300 µm 350 µm 400 µm	25 µm	s = 100 µm, t = 50 µm

(b)

Length, L	Leg width, b,	Diaphragm,
250 µm 300 µm 350 µm	25 µm	s = 100 µm, t = 70 µm

(c)

Fig. 8. Microbeam dimensions: (a) straight beam for SA and SB devices, (b) H-beam for HA and HB devices, (c) H-beam for HO devices. Beam thickness is set to 2.1 μm.

Table 1
Driving and sensing electrode sizes of the resonant beam devices.

HO	HA	HB	SA	SB
Driving electrode	Driving electrode	Driving electrode	Driving electrode	Driving electrode
~100×80 μm^2	~100×10 μm^2	~100×100 μm^2	~20×56 μm^2	~170×56 μm^2
Sensing electrode	Sensing electrode	Sensing electrode	Sensing electrode	Sensing electrode
~100×80 μm^2	~100×60 μm^2	~100×100 μm^2	~120×56 μm^2	~Beam length×56μm^2

5. Fabrication Process

The micromachined resonating beams are fabricated with a thirteen-mask process. The process starts by defining the reference alignment marks on a (111), n-type silicon wafer by patterning photoresist with the first mask (#1) and etching the silicon. The first electronic elements, the driving and sensing electrodes are defined with the second mask (#2). The photoresist defined by the second mask is used for a boron implant with a dose of 2×10^{15} cm^{-2} and an energy of 80 keV. Subsequent drive-in at 980°C after growing 0.01 μm of silicon dioxide activates the implanted boron impurities and forms boron diffused layers embedded in the n-type silicon substrate. The purpose of the thin silicon dioxide is to prevent out-diffusion during the drive-in and, therefore, the loss of boron impurities at the surface. The drive-in time influences the junction depth and the lateral diffusion width, which must be controlled by the design criteria for electronic circuits. The next step is to define the ground planes using the third mask (#3). A phosphorous implant is used for the ground planes since the substrate is n-type. The implantation is performed with a dose of 5×10^{15} cm^{-2} and an energy of 100 keV. This results in good ohmic contact with the metal. The process continues with the growth of 0.03 μm silicon dioxide followed by 0.09 μm of low stress LPCVD silicon nitride. This step also results in another drive-in for the boron and phosphorus impurities and, therefore, this step must also be taken into account when designing the electronic circuitry in the silicon substrate. The cross-sectional view of the device after this step is shown in Fig. 9(a). The silicon dioxide and silicon nitride films are patterned with the fourth mask (#4) to open areas for the first sacrificial wells. The layers are etched with a NF_3 plasma using a photoresist mask. The remaining stencil of the silicon nitride acts as an oxidation barrier for the underlying silicon. This type of selective oxidation is known as the local oxidation of silicon (LOCOS) process, which has been widely used for isolation in microelectronics. The first oxidation of the cavity well areas is performed to produce 0.85 μm of silicon dioxide, which consumes approximately 0.425 μm of silicon measured from the surface, as shown in Fig. 9(b). This silicon dioxide well are called the "active area." The other region is called the "field area." The silicon dioxide wells are then removed with buffered HF, leaving empty wells surrounded by a silicon nitride field. The second oxidation of the empty wells is performed to obtain a planar surface. This requires about 0.85 μm of silicon dioxide to be grown. Since about 0.425 μm of silicon on the cavity areas is consumed during the first oxidation, the resulting surface of silicon dioxide is now coplanar with the silicon surface after the second oxidation.

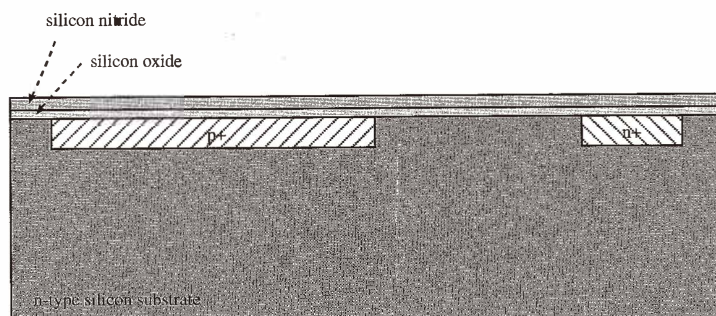

Fig. 9(a). Cross-sectional view after substrate electronics. The structures of the silicon dioxide and silicon nitride for the LOCOS process are defined.

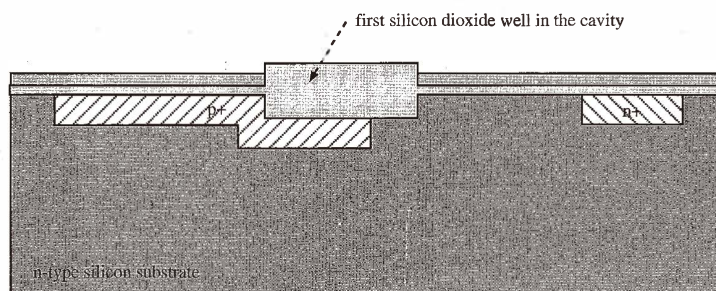

Fig. 9(b). Formation of the lower sacrificial layer by the LOCOS process: the first oxidation.

Nominal planarity between these two surfaces can be controlled to 0.1 μm. Figure 9(c) shows the cross-sectional view of the device after the second oxidation for cavity formation has been carried out. A NF_3 plasma etch of the silicon dioxide and silicon nitride in the field areas patterned with photoresist using the fifth mask (#5) produces the etch channels.[4, 9] These etch channels are used for etching the silicon dioxide and silicon nitride surrounding the polysilicon beam in the cavity once the polysilicon encapsulating cover is deposited. Since the relative etch rate of silicon nitride to silicon dioxide is about 5:1, the silicon nitride can be overetched to ensure that the field area is cleared. Next, the beam polysilicon is deposited by LPCVD at 590°C to a thickness of 2 μm. Boron implantation with a dose of 2×10^{15} cm^{-2} and an energy of 80 keV is performed on the beam polysilicon areas, which are defined using the sixth mask (#6). The subsequent annealing at 825°C for

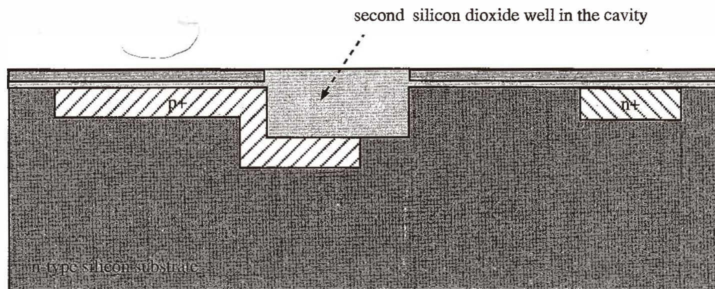

Fig. 9(c). Formation of the lower sacrificial layer by oxidizing the opened silicon substrate by the LOCOS process. The second oxidation after removing the initially grown oxide is used to achieve planarity.

3 h causes the implanted boron impurities to diffuse into the polysilicon. This ensures that the patterned beam polysilicon is uniformly doped and acts as a good conductor. The annealing at 825°C for 3 h also produces a built-in tensile strain of about 0.2%, which prevents buckling when freeing the beam. The beam polysilicon is patterned using the seventh mask (#7). The opened areas of the beam polysilicon are then etched by a NF_3 plasma, which produces the beam shapes on the active areas. Opening contact areas for electronic circuitry in the silicon substrate is also performed at this time. Since the etch method is reactive ion etching (RIE), the resulting beam flanks are nearly vertical. Figure 9(d) shows the cross-sectional view of the device at this step. The process continues with the deposition of the upper sacrificial layer. This 0.85-μm-thick, low stress, silicon nitride film is deposited by LPCVD at 825°C and followed by a 0.2-μm-thick LPCVD polysilicon deposition at 590°C. The upper sacrificial layer can also be formed with a low stress, tensile, densified silicon dioxide. This process is being used at the Honeywell Technology Center[6,10] using a low temperature oxide deposition method. The thin polysilicon on the silicon nitride upper sacrificial layer is used as a protection layer when the upper sacrificial layer, the spacer, is defined. Patterning of the upper sacrificial layer on the beam polysilicon is performed by a NF_3 plasma etch using the eighth mask (#8). Since the plasma etching leaves a rough and non-uniform surface on the etched area, the sacrificial layers must not be etched completely. The remaining sacrificial material is then etched with phosphoric acid at 180°C after removing the photoresist, which keeps a smooth polysilicon surface in the field and active areas. As mentioned earlier, the thin polysilicon in the spacer areas protects the underlying silicon nitride sacrificial layer from being etched in the H_3PO_4 acid. Figure 9(e) shows the patterned LPCVD silicon nitride and the lower silicon dioxide well which together completely surround the doped polysilicon beam. LPCVD polysilicon is deposited next at 590°C. This polysilicon covers the entire surface of the silicon wafer. A subsequent annealing at 825°C for 3 h is performed to prevent damage to the covered polysilicon when freeing the beams. Photoresist is patterned with the ninth mask (#9). A NF_3 plasma etch is then used to open the etch channels and the beam

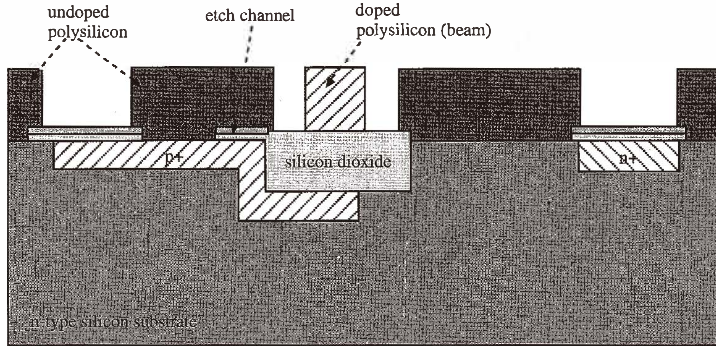

Fig. 9(d). Cross-sectional view of the doped beam over the silicon dioxide well. The etch channels are also defined.

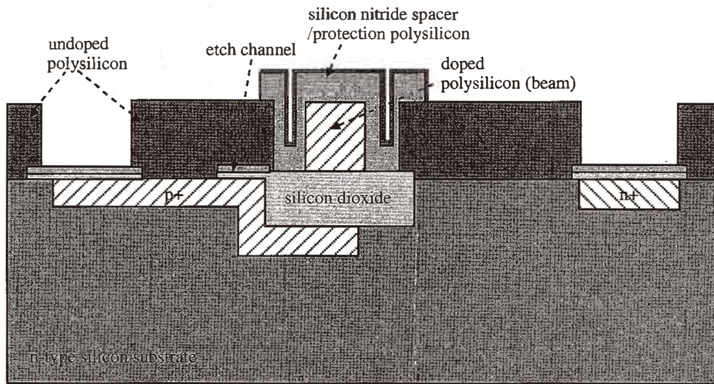

Fig.9(e). The patterned LPCVD silicon nitride and the lower silicon dioxide well completely surround the doped polysilicon beam and are used as removable sacrificial layers.

contact areas, as shown in Fig. 9(f). The wafer is now ready for the sacrificial layer etch. The etch time depends on the etch rate of the sacrificial layer and the size of the cavity area. The etch rate in HF diluted by DI water in the ratio of 1 to 1 of the silicon nitride is about 0.01 μm/min. A 65-h immersion in this etch removes all the sacrificial layers in this design. Overetching is possible since the etch is self-limiting. The process continues with rinsing in DI water to remove HF from the surface of the wafer. The final rinse is then performed with ethanol and then cyclohexane followed by the freeze and sublimation process, leaving free-standing beams in the cavities. The cavity sealing process is accomplished by a 0.4 μm deposition of the LPCVD polysilicon followed by 0.1 μm

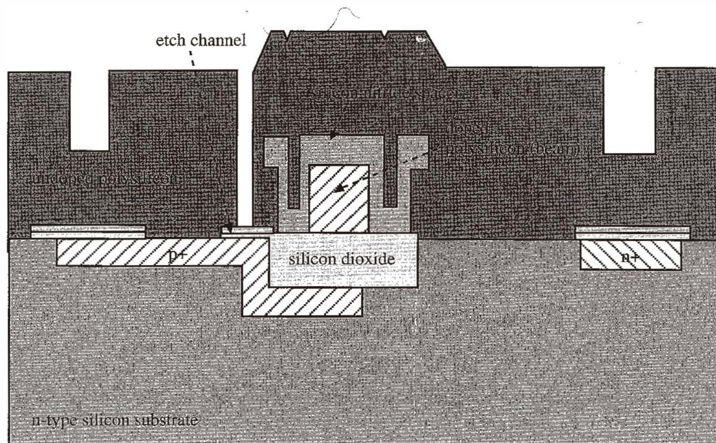

Fig. 9(f). The polysilicon has been patterned and etched to expose the etch channel to the interior of the cavity after covering the entire surface with polysilicon.

deposition of the LPCVD silicon nitride.[4,7] Using the masks (#10, 11, 12), the contact openings over the pad areas are formed with proper isolation of the local areas for electronics. The thin LPCVD silicon nitride film is used for this isolation. A 98% aluminum, 1% silicon, 1% copper alloy is sputtered to form a 0.65-μm-thick metal film, followed by a 30 minute metal alloying in 10% H_2/90% N_2 forming gas at 480°C. To complete the process, the metal is patterned with the final mask (#13). The metal etching is performed with a defreckling aluminum etchant.[13] The metal patterns provide bonding pads connected to the electronics and the upper electrodes. Figure 9(g) shows the cross-sectional view of a completed planar processed microbeam device.

Figure 10 shows the SEM photographs of two-port devices with two separate electrodes (p-diffused layer and metal) in the beam resonator (SB and HB). The metal electrode formed on the polysilicon cover is clearly visible in Fig. 10.

6. Experimental Results

Dynamic mechanical responses such as resonant frequency and quality factor have been measured on the devices. It is possible to measure the dynamic response of microbeams on the wafers using the optical detection method[5,6,14] which employs laser optics for sensing and an acoustic vibrator for driving the beam. Figure 11 shows the experimental set-up for the optical detection method.

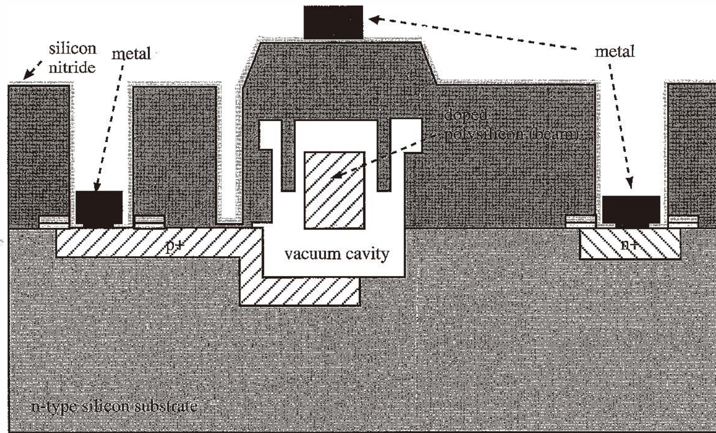

Fig. 9(g). Cross-sectional view of a completed planar processed microbeam device. The metallization connects the bonding pads to the p^+ regions, the n ground, and the electrode located on the polysilicon cover.

6.1 *Resonant frequency*

The resonant frequencies of HO, HA and SA microbeam devices were measured using the optical detection method. The measurements of SB and HB devices by the optical detection method cannot be performed since there are metal electrodes on the vacuum sealed microcavities which contain the resonant beams. A typical measurement result from the HP4194A gain-phase analyzer using the optical detection method is shown in Fig. 12. The maximum gain occurs at resonance and the phase change going through resonance is 180°. The ranges of the measured resonant frequencies of HO, HA and SA devices are given in Table 2. The uniformity of the resonant frequencies for each device type is about 10%. The results may be an indication of the uniformity of the polysilicon film used for the beams since the resonant frequency of a microbeam is proportional to the beam thickness.[4,7,14]

6. 2 *Quality factor*

Quality factors of the resonant microbeams are measured by gain-phase spectra using the definition of the quality factor

$$Q = \frac{w_R}{w_2 - w_1} = \frac{f_R}{f_2 - f_1}, \tag{3}$$

where f_1 and f_2 are the frequencies at which the amplitudes are $0.707X_{res}$. The value of X_{res} is the amplitude at resonance. Figure 12 shows the gain-phase spectrum of a beam

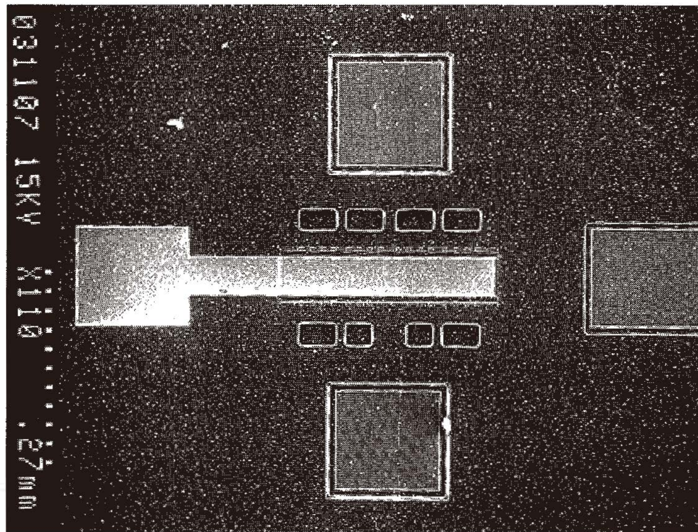

(a)

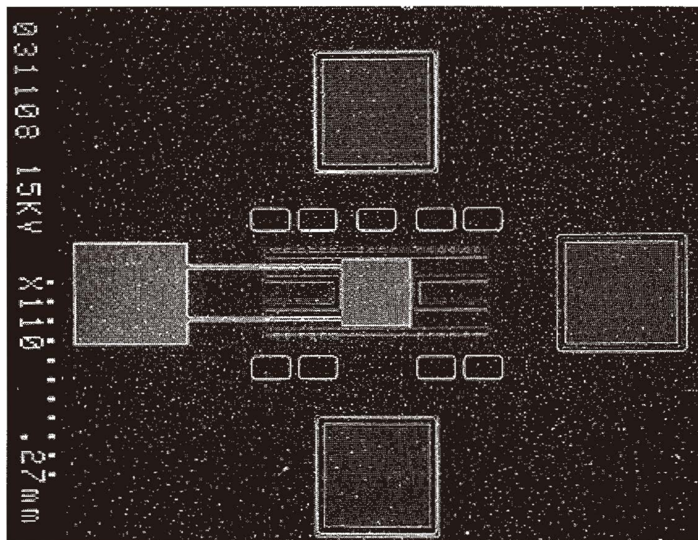

(b)

Fig. 10. SEM photographs of SB and HB devices: (a) SB ~length L=300 μm, width W =56 μm, and (b) HB ~ length L=300 μm, leg width b=25 μm. The diaphragm size is 100 $\times$ 100 μm^2.

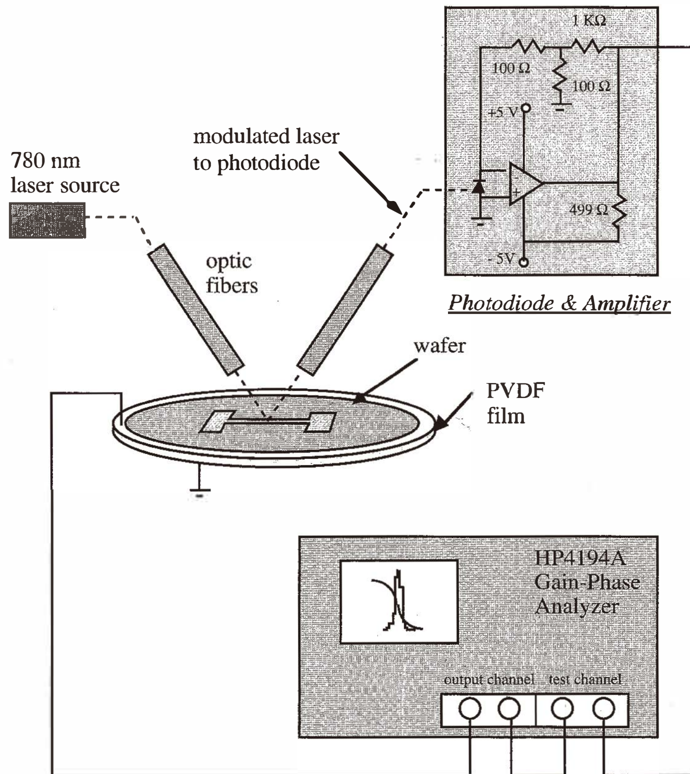

Fig.11. Measurement set-up for optical detection method.

resonator with a measured Q of greater than 300,000. The measured Q ranges for HO, HA and SB devices are shown in Table 3. The data indicate that polysilicon sealed-cavity resonators can have high Qs. However, there is a large variability in Q. The reasons for this are not known at the present time. The results also indicate that the microbeams with longer lengths and shorter widths have larger Qs. The Qs of H-beams which have short leg widths are larger than those of straight beams. The longer beams have large Qs. This can be explained by the support-related losses which can be estimated by assuming that the supports radiate acoustic energy into a semi-infinite silicon substrate.(10) The situation is similar to the case of a freely vibrating string fixed at one end and attached at the other end to a dashpot which can move transversely, a system of which has been analyzed by Kinsler *et. al.*(15) The equation for the support-related Q of rectangular microbeams with a cross-sectional area, A_b(10,14) is

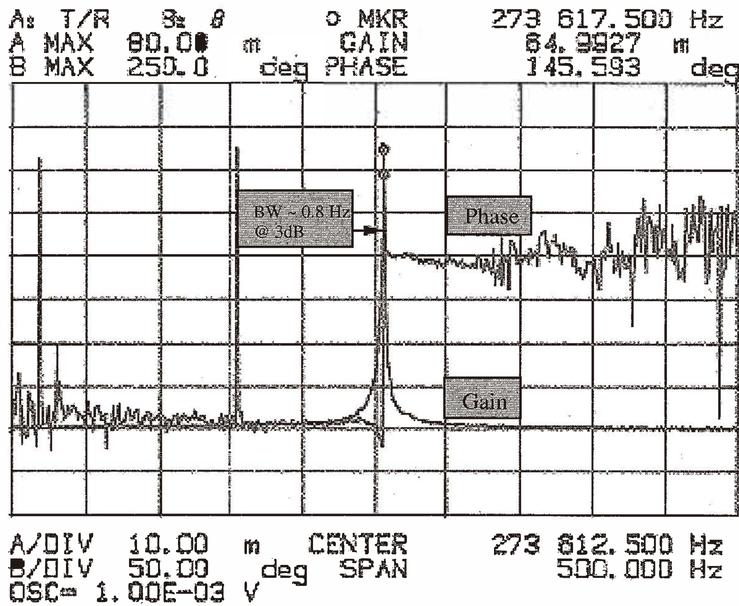

Fig. 12. Gain-phase spectrum of an HA device shows that the measured Q is greater than 300,000 and the measured resonant frequency is about 273.6175 kHz. Beam dimensions: Length $L = 350$ μm, leg width $W = 25$ μm. The diaphragm size is 100×100 μm^2 and the beam thickness $h = 2.1$ μm.

Table 2
The resonant frequency ranges of HO, HA and SA devices.

HO		HA		SA	
L/b	f_R	L/b	f_R	L/W	f_R
250/25 μm	380–404 kHz	300/25 μm	309–330 kHz	300/56 μm	400–435 kHz
300/25 μm	293–319 kHz	350/25 μm	257–286 kHz	400/56 μm	275–300 kHz
350/25 μm	246–280 kHz	400/25 μm	221–243 kHz	500/56 μm	215–235 kHz

$$Q = \frac{2\pi cm / \rho}{\omega_R A_b^2} = \frac{cL}{f_R W h}, \tag{4}$$

where m is the beam mass, ρ is the material density, c is $\sqrt{E/\rho}$, E is the Young's modulus, L is the beam length, W is the beam width (the leg width, b, for an H-beam), and h is the beam thickness. Equation (4) predicts that Q increases with increasing length-to-width

Table 3
Measured Q ranges for HO, HA and HB devices.

HO			HA			SA		
L/b	Q	Q_{max}	L/b	Q	Q_{max}	L/W	Q	Q_{max}
250/25 μm	>30,000	40,000	300/25 μm	>20,000	200,000	300/56 μm	>10,000	50,000
300/25 μm	>30,000	70,000	350/25 μm	>15,000	300,000	400/56 μm	>10,000	70,000
350/25 μm	>30,000	150,000	400/25 μm	>15,000	200,000	500/56 μm	>10,000	80,000

ratio and with decreasing thickness and frequency. The trends in Q displayed in Table 3 are in agreement with eq. (4). It can be concluded that the support-related losses are a significant parameter for vacuum encapsulated microbeams.

7. Conclusion

Surface micromachining technology can be used to fabricate micromechanical resonating beams and integrated electronic circuitry. Micromechanical beam structures can be made from polysilicon by etching the surrounding sacrificial layers in buffered or concentrated HF. These beams are encased in vacuum cavities in which the vacuum has been chemically induced by the reactive sealing process. Because of this the beams have high mechanical Q. High-temperature annealing reduces the internal strain in the polysilicon film. The sublimation process enables longer free-standing microbeams to be made. Since the surface micromachining process uses only standard electronic materials, cofabrication of microbeams and electronic circuits is possible.

Acknowledgments

The authors thank Dr. J. D. Zook at the Honeywell Technology Center for valuable discussions and the staff of the Wisconsin Center for Applied Microelectronics for technical assistance.

References

1 J. D. Zook, D. W. Burns, H. Guckel, J. J. Sniegowski, R. L. Engelstad and Z. Feng: Sensors and Actuators A **35** (1992) 51.
2 H. Guckel: Sensors and Materials, **4**(5) (1993) 251.
3 H. Guckel, M. Nesnidal, J. D. Zook and D. W. Burns: Transducers '93, Proc. of 7th Intl. Conf. on Solid-State Sensors and Actuators, Yokohama, Japan, p. 686.
4 J. J. Sniegowski: Ph.D. Thesis, University of Wisconsin-Madison, USA, Dec., 1991.
5 J. D. Zook, D. W. Burns, J. N. Schoess and H. Guckel: SPIE Proc. Vol. 2383**A**, Conf. Miniaturized Systems with Micro-optics and Micromechanics, Photonics 1995, San Jose, CA, USA, February 1995.

6 J. D. Zook , D. W. Burns, W. R. Herb, H. Guckel, J. W. Kang and Y. Ahn: Sensors and Actuators A **52** (1996) 92.
7 J. W. Kang: Ph.D. Thesis, University of Wisconsin-Madison, USA, May, 1996.
8 H. Guckel and D. W. Burns: IEDM Digest, 1984, p. 223.
9 D. W. Burns: Ph. D. Thesis, Dept. Mat. Sci., UW-Madison, U.S.A. 1988.
10 J. David Zook, William R. Herb, Y. Ahn and Henry Guckel: J. Vac. Sci. & Technol. A **17**(4), Jul/Aug (1999) 2286.
11 H. Guckel, D. W. Burns, C. C. G. Visser, H. A. C. Tilmans and D. Deroo: IEEE Trans. on Electron Devices, ED-**35** (1988) 800.
12 K. Ikeda, H. Kuwayama, T. Kobayashi, T. Watanabe, T. Nishikawa, T. Yoshida and K. Harada: Proc. of the 5th Intl. Conf. Solid-State Sensors and Actuators and Eurosensors III, Vol. **2**, June 25–30, 1989, p. 146.
13 Defreckling Aluminum Etchant (DAE), Technical data from Arch Chemicals Corp.
14 Y. Ahn: Ph.D. Thesis, University of Wisconsin-Madison, USA, 1999.
15 L. E. Kinsler, A. R. Ferry, A. B. Coppens and J. V. Sanders: Fundamentals of Acoustics, 3rd Edition, John Wiley & Sons, 1982, p.51.